Available online at www.sciencedirect.com

ScienceDirect

Journal of Power Sources 179 (2008) 186–199

JOURNAL OF POWER SOURCES

www.elsevier.com/locate/jpowsour

A three-dimensional agglomerate model for the cathode catalyst layer of PEM fuel cells

Prodip K. Das [a], Xianguo Li [a,*], Zhong-Sheng Liu [b]

[a] *Department of Mechanical Engineering, University of Waterloo,*
200 University Avenue West, Waterloo, ON, Canada N2L 3G1
[b] *Institute for Fuel Cell Innovation, National Research Council, Vancouver, BC, Canada V6T 1W5*

Received 14 October 2007; received in revised form 16 December 2007; accepted 18 December 2007

Abstract

In this work, a three-dimensional, steady-state, multi-agglomerate model of cathode catalyst layer in polymer electrolyte membrane (PEM) fuel cells has been developed to assess the activation polarization and the current densities in the cathode catalyst layer. A finite element technique is used for the numerical solution to the model developed. The cathode activation overpotentials, and the membrane and solid phase current densities are calculated for different operating conditions. Three different configurations of agglomerate arrangements are considered, an in-line and two staggered arrangements. All the three arrangements are simulated for typical operating conditions inside the PEM fuel cell in order to investigate the oxygen transport process through the cathode catalyst layer, and its impact on the activation polarization. A comprehensive validation with the well-established two-dimensional "axi-symmetric model" has been performed to validate the three-dimensional numerical model results. Present results show a lowest activation overpotential when the agglomerate arrangement is in-line. For more realistic scenarios, staggered arrangements, the activation overpotentials are higher due to the slower oxygen transport and lesser passage or void region available around the individual agglomerate. The present study elucidates that the cathode overpotential reduction is possible through the changing of agglomerate arrangements. Hence, the approaches to cathode overpotential reduction through the optimization of agglomerate arrangement will be helpful for the next generation fuel cell design.

Keywords: Agglomerate; Cathode catalyst layer; PEM fuel cell; Polarization; Three-dimensional modeling

---

1. Introduction

Polymer electrolyte membrane (PEM) fuel cell is a promising candidate for the next generation power sources due to its high power density, low operating temperature, quick start-up, and fast dynamic response. Most importantly, its zero emission capabilities open up opportunities to wide practical use in portable, mobile, and stationary cogeneration applications [1]. Even though substantial improvements have been made over the past few years in the cell design and material utilization in PEM fuel cells, several technical barriers still exist that prevent the PEM fuel cells from commercialization. Among the various obstacles, the most important are low cell performance due to high polarization, and high cost due to platinum (Pt) catalyst used in the catalyst layer (CL). Hence, there has been considerable interest in the modeling and optimization of PEM fuel cells aiming at performance improvement and cost reduction [2–17].

The performance of a PEM fuel cell is mainly dictated by ohmic, activation, and concentration overpotentials. At the most common operating ranges, ohmic and activation overpotentials are dominant over the concentration overpotential, or simply existence of concentration overpotential is negligible. The estimation of the ohmic overpotential has already been well-established that can be determined from the available experimental data or from the empirical relation for the cell polarization curve of PEM fuel cells [6–8,11,18]. On the other hand, the activation overpotential shows more complex nature due to its dependency on the catalyst layer structure; for instance, whether it has agglomerate or macro-homogeneous structure, composition of the catalyst layer, types of the catalysts used,

---

[*] Corresponding author. Tel.: +1 519 888 4567x36843.
E-mail address: x6li@uwaterloo.ca (X. Li).

0378-7753/$ – see front matter © 2007 Elsevier B.V. All rights reserved.
doi:10.1016/j.jpowsour.2007.12.085

and how the reactants transport in the catalyst layer. Therefore, activation overpotential cannot be estimated easily. Furthermore, activation overpotential in the anode catalyst layer is very small compared to the activation overpotential in the cathode catalyst layer; hence, the activation overpotential in the cathode catalyst layer has major influence on the cell performance. Among the various catalyst layer models investigated, three different models of cathode catalyst layer have been established in the past decade, namely, thin-film, macro-homogeneous, and agglomerate model. In the thin-film model, the catalyst particles are embedded on the thin-film of polymer membrane [19,20]; whereas in the macro-homogeneous model, the cathode catalyst layer is considered as a homogeneous matrix of supported catalyst platinum, polymer electrolyte, and void spaces [4,5,9,10]. In the agglomerate model, the catalyst layer is considered as a uniform matrix of catalyst agglomerates, which is surrounded by the gas pores. Each of these catalyst agglomerates are assumed to be homogeneous mixture of catalysts, polymer electrolytes, and void spaces as well [15,21–27]. In addition, there are several other models that have also been developed, namely, cylindrical agglomerate [28], ordered catalyst layer [29], and non-uniform catalyst layer [30]. It should be noted here that experimental studies showed that the agglomerate model might be a close approximation to model the catalyst layer for PEM fuel cells [22,31].

On the other hand, in terms of the computational efficiency in numerical modeling, three different approaches to catalyst layer modeling would be more viable. In a most simplified approach, the catalyst layer is considered as an ultra-thin layer between the membrane and gas diffusion layer (GDL), ignoring the reaction kinetics and transport processes within the catalyst layer [32]. This is useful, particularly for the three-dimensional full cell model due to the limited computing power. Hence, the catalyst layer is assumed as a source or sink boundary condition that is simple to implement for predicting the typical polarization curve, optimizing the cell design parameters, and operating conditions. In the second approach, the catalyst layer is considered as more realistic thin layer of catalyst particles and electrolyte membrane or the agglomerate of catalyst particles and electrolyte membrane sandwiched between the membrane and gas diffusion layer [4,5,9,10,15,23–25,30,33]. All of these studies used the one-dimensional approach for the catalyst layer or for the individual catalyst agglomerate. Recently, two-dimensional model results are presented for the agglomerate model [27]. Once again, the individual agglomerate is accounted by considering diffusion in the radial direction only. However, to improve the performance of the cathode catalyst layer and reduce the cost associated with the Pt-catalyst, it is required to study transport processes in the cathode catalyst layer. Furthermore, transport processes in the cathode catalyst layer are largely depend on the structures of the catalyst layer or the arrangements of catalyst agglomerates in the cathode catalyst layer. Therefore, the third and most practical approach would be detailed modeling of the cathode catalyst layer using three-dimensional approach. None of the previous studies has reported the three-dimensional nature of the agglomerate catalyst layer that would be an accurate approximation of a practical catalyst layer.

In this study, a three-dimensional (3D) agglomerate model of cathode catalyst layer in a PEM fuel cell is developed to study the activation overpotential in the cathode catalyst layer. The effect of agglomerate arrangements on the activation overpotential of PEM fuel cells has been investigated for three different types of agglomerate arrangements, namely, in-line agglomerate arrangement as Case-I, and two staggered agglomerate arrangements as Case-II and Case-III. The catalyst layer geometry is generated assuming that the agglomerates are aligned along the thickness of the catalyst layer in the first case and then by considering staggered arrangements in the subsequent cases. Since the governing equations are nonlinear partial differential equations and the catalyst layer has a complex geometry, finite element technique is used to solve the governing equations due to its ability to handle complex geometrical domains [34,35]. The simulation results presented here show a considerable insight on how the activation overpotential changes with the arrangement of catalyst agglomerates that will eventually be helpful for the better understanding of PEM fuel cell performance and its design.

2. Model description

A typical PEM fuel cell is considered that consists of a cathode and an anode electrode with a proton conducting membrane as the electrolyte sandwiched in between. Generally, the thickness of the electrodes and membrane are approximately 250 μm. Each of these electrodes also consists of approximately 10 μm (or thinner) catalyst layer between the electrode and the membrane, known as the anode catalyst layer and cathode catalyst layer, respectively. Typically, humidified H_2 gas is supplied under pressure into the anode flow channel which diffuses through the porous electrode until it reaches the anode catalyst layer and forms protons (H^+) and electrons via electro-oxidation reaction at the catalyst surface. The protons are transferred through the membrane to the cathode catalyst layer, and the electrons are transported via the external circuit to the cathode. Conversely, humidified O_2 gas or air is supplied to the cathode flow channel where O_2 gas diffuses through the porous electrode until it reaches the cathode catalyst layer and forms water reacting with protons and electrons. The overall electro-chemical reaction occurring in the PEM fuel cell can be represented by the following reaction:

$$\mathrm{H_2} + \frac{1}{2}\mathrm{O_2} \rightarrow \mathrm{H_2O} + \text{Heat} + \text{Electric energy} \tag{1}$$

2.1. Governing equations

In this study, a three-dimensional modeling domain is considered, which is geometrically identical to our previous study [18], except the catalyst layer structure. A schematic diagram of the cathode catalyst layer under consideration is shown in Fig. 1. Here, the catalyst agglomerates are considered as a homogeneous mixture of electrolyte membrane, supported Pt-catalyst, and void space. The volume fractions of these components can be varied as can the effective surface area of catalyst that can

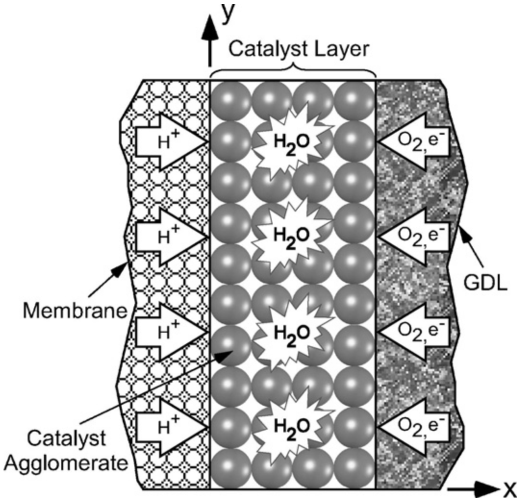

Fig. 1. Schematic of the cathode catalyst layer in a PEM fuel cell.

be characterized by different loadings and catalyst types. The overall reaction in the catalyst agglomerate is taken as

$$O_2 + 4H^+ + 4e^- \rightarrow 2H_2O \tag{2}$$

Assuming the cell is operating in steady-state condition and the membrane is fully humidified, the conservation equation for oxygen in the cathode catalyst layer (inside the agglomerates) can be written as

$$\nabla \cdot \left(D_{O_2}^{\text{eff}} \nabla C_{O_2} \right) + \Re_{\text{orr}} = 0 \tag{3}$$

where $D_{O_2}^{\text{eff}}$ is the effective diffusion coefficient of the transported oxygen that is calculated using Bruggeman correction from the bulk diffusion coefficient, D_{O_2}, and the corresponding void fraction, ϕ_i as [36]

$$D_{O_2}^{\text{eff}} = \phi_i^{3/2} D_{O_2} \tag{4}$$

Since there is no reaction outside the agglomerates, the oxygen reduction reaction rate or the rate of electro-chemical reaction ($\Re_{\text{orr}}$) is equal to zero outside the agglomerates in Eq. (3); therefore, diffusion is the mechanism for oxygen transport in the void region outside the agglomerates. Conversely, the oxygen reduction reaction rate inside the agglomerates is given by the Butler–Volmer equation as [1]

$$\begin{aligned} \Re_{\text{orr}} = \frac{A_v J_{0,\text{ref}}}{n\Im} \left(\frac{C_{O_2}}{C_{O_2,\text{ref}}} \right)^{\gamma} \Bigg\{ & \exp\left(\frac{\alpha_a n \Im \eta_{\text{act}}}{\Re T} \right) \\ & - \exp\left(-\frac{\alpha_c n \Im \eta_{\text{act}}}{\Re T} \right) \Bigg\} \end{aligned} \tag{5}$$

Here, the catalyst reactive surface area per unit volume (A_v) is a function of the catalyst mass loading per unit area of cathode (m_{Pt}), the catalyst surface area per unit mass of the catalyst (A_s), and the thickness of the catalyst layer (δ_c), which is calculated using the following relation [18]:

$$A_v = \frac{A_s m_{\text{Pt}}}{\delta_c} \tag{6}$$

The reference current density ($J_{0,\text{ref}}$) at the reference concentration of $C_{O_2,\text{ref}}$ is calculated using the experimental data of Parthasarathy et al. [38] and the reference oxygen concentration, $C_{O_2,\text{ref}}$, is taken as 1.2 mol m^{-3}[10,38]. The experimental data of the reference exchange current density in A cm^{-2} for oxygen reduction in Nafion® were correlated with the cell temperature in Kelvins by [10]

$$\log_{10}(J_{0,\text{ref}}) = 3.507 - \frac{4001}{T} \tag{7}$$

In Eq. (5), γ is the overall reaction order, α_a and α_c are the apparent transfer coefficients for the anodic and cathodic reactions, respectively, and η_{act} represents the activation overpotential for the electro-chemical reactions.

It is assumed that the electric current flowing through the catalyst layer obeys the Ohm's law, which relates the electrical current density to the potential gradient as

$$J_i = -\sigma_i^{\text{eff}} \nabla \Psi_i \tag{8}$$

where σ_i^{eff} is the effective conductivity of the medium through which the current travels and index i refers the phases in the catalyst layer. Since the catalyst agglomerate in the catalyst layer consists both the electrolyte membrane phase and the solid catalyst, Eq. (8) can be written for the catalyst agglomerates as

$$J_m = -\sigma_m^{\text{eff}} \nabla \Psi_m \quad \text{for membrane phase current} \tag{9}$$

$$J_s = -\sigma_s^{\text{eff}} \nabla \Psi_s \quad \text{for solid phase current} \tag{10}$$

where J_m and J_s are the membrane phase current density and the solid phase current density, σ_m^{eff} and σ_s^{eff} are the effective protonic conductivity of the membrane and the effective electronic conductivity of the carbon support in the agglomerate, Ψ_m and Ψ_s are the membrane potential and the solid phase potential, respectively. In addition, the current conservation equation yields [37]

$$\nabla \cdot J_m + \nabla \cdot J_s = 0 \tag{11}$$

In the cathode catalyst layer, the protonic current is defined as the flow of positively charged particles and the electronic current is defined as the flow of negatively charged particles. Since the flow of electrons depends on the flow of oxygen in the cathode catalyst layer through Eq. (2), the relationship between the solid phase current and the oxygen reduction reaction rate can be related as

$$\nabla \cdot J_s = -n\Im\Re_{\text{orr}} \tag{12}$$

where n is the number of electrons transferred in the cathodic reaction in Eq. (2).

By combining Eqs. (9)–(12), the membrane phase potential and the solid phase potential equations within the catalyst agglomerates are summarized as follows:

$$\nabla \cdot \left(\sigma_m^{\text{eff}} \nabla \Psi_m \right) = -n\Im\Re_{\text{orr}} \quad \text{for membrane phase potential} \tag{13}$$

$$\nabla \cdot \left(\sigma_s^{\text{eff}} \nabla \Psi_s \right) = n\Im\Re_{\text{orr}} \quad \text{for solid phase potential} \tag{14}$$

where $\sigma_{\mathrm{m}}^{\mathrm{eff}}$ and $\sigma_{\mathrm{s}}^{\mathrm{eff}}$ within the catalyst agglomerates are calculated with Bruggemann correction from the bulk conductivity using the following expressions:

$$\sigma_{\mathrm{m}}^{\mathrm{eff}} = \sigma_{\mathrm{m}}(l_{\mathrm{m}} \times \phi_{\mathrm{c}})^{3/2} \tag{15}$$

$$\sigma_{\mathrm{s}}^{\mathrm{eff}} = \sigma_{\mathrm{s}}(1 - \phi_{\mathrm{c}})^{3/2} \tag{16}$$

where l_{m} denotes the volume fraction of membrane in the agglomerates, σ_{m} and σ_{s} are the bulk conductivities of the membrane and the solid catalyst, respectively, and ϕ_{c} is the void fraction in the agglomerates.

2.2. Boundary conditions

The overpotential in the cathode catalyst layer is defined as the potential difference between the local value and the reference potential. In order to be able to calculate the overpotential in the cathode catalyst layer, it is required to define a reference potential in the catalyst layer. In the present model, the solid phase potential is considered as the reference potential that eventually simplified the electronic overpotential as zero and the protonic overpotential as the total activation overpotential. Hence, the activation potential in the cathode catalyst layer is simplified to

$$\eta_{\mathrm{act}} = \Psi_{\mathrm{s}} - \Psi_{\mathrm{m}} \tag{17}$$

Furthermore, following boundary conditions are used to solve the governing partial differential equations. For the oxygen transport equation, the boundary conditions are defined as

$$C_{\mathrm{O_2}} = C_{\mathrm{int}} \quad \text{for } \partial\Omega \in \text{ GDL–CL interface} \tag{18a}$$

$$\nabla C_{\mathrm{O_2}} = 0 \quad \text{for } \partial\Omega \in \text{ membrane–CL interface} \tag{18b}$$

$$\mathbf{n}.(\mathbf{N}_{\mathrm{in}} - \mathbf{N}_{\mathrm{out}}) = 0$$
$$\text{for } \partial\Omega \in \text{ agglomerate–void space interface} \tag{18c}$$

where C_{int} is the oxygen concentration at the GDL–CL interface, $\partial\Omega$ represents the boundary of the computational domain, and $\mathbf{n}$ is the unit normal vector. $\mathbf{N}_{\mathrm{in}}$ and $\mathbf{N}_{\mathrm{out}}$ represent the inward and outward fluxes at the agglomerate–void space interface, respectively, that is defined as

$$\mathbf{N}_i = -D_i \nabla (C_{\mathrm{O_2}})_i \tag{19}$$

where index i refers inward or outward direction. The calculation of C_{int} is not trivial since oxygen concentration is normally known in the flow channel, and decreases after transporting through the GDL to reach the catalyst layer. However, an appropriate measure is required at the liquid–gas interface for partially flooded agglomerates in the catalyst layer since the reactant gas is weakly soluble in liquid water under the typical fuel cell operating condition, Henry's law can be used to relate the reactant concentrations in the gas and liquid phases. The details are given in our earlier work [18]. For the membrane phase potential, the boundary conditions are

$$\nabla \Psi_{\mathrm{m}} = 0 \quad \text{for } \partial\Omega \in \text{ GDL–CL interface} \tag{20a}$$

$$-\sigma_{\mathrm{m}}^{\mathrm{eff}} \nabla \Psi_{\mathrm{m}} = J_{\mathrm{m}} \quad \text{for } \partial\Omega \in \text{ membrane–CL interface} \tag{20b}$$

$$\mathbf{n}.J_{\mathrm{m}} = 0 \quad \text{for } \partial\Omega \in \text{ agglomerate–void space interface} \tag{20c}$$

where J_{m} is the membrane current density at the membrane–CL interface. Finally, for the solid phase potential as

$$-\sigma_{\mathrm{s}}^{\mathrm{eff}} \nabla \Psi_{\mathrm{s}} = J_{\mathrm{s}} \quad \text{for } \partial\Omega \in \text{ GDL–CL interface} \tag{21a}$$

$$\Psi_{\mathrm{s}} = 0 \quad \text{for } \partial\Omega \in \text{ membrane–CL interface} \tag{21b}$$

$$\mathbf{n}.J_{\mathrm{s}} = 0 \quad \text{for } \partial\Omega \in \text{ agglomerate–void space interface} \tag{21c}$$

where J_{s} is the solid phase current density at the GDL–CL interface. Due to the geometric symmetry, the total membrane current density at the membrane–CL interface is equal to the total solid phase current density at the GDL–CL interface, i.e.,

$$J_{\mathrm{m}} \in \text{membrane–CL interface} = J_{\mathrm{s}} \in \text{GDL–CL interface} = J_{\delta} \tag{22}$$

where J_{δ} is the boundary value of the current densities for the two interfaces as mentioned above. In addition to the above-mentioned boundary conditions, insulation or symmetry boundary conditions are applied in the appropriate boundaries when required.

2.3. Operating conditions and physical parameters

In the present investigation, it is considered that air is the cathode gas and the concentration of oxygen in the cathode flow channel is uniform. The electrode is considered dry; hence, the oxygen diffuses through the un-flooded electrode void region to reach the GDL–CL interface. In addition, the catalyst agglomerates are considered partially hydrated and water in the void region around the agglomerates is considered in gaseous phase to simulate the un-flooded scenarios and the start-up case. The thickness of the catalyst layer in the present study is considered as 10 μm and the agglomerate diameter is considered as 5 μm. Typically, the thickness of the catalyst layer and the agglomerate size depend on the amount of catalyst loading and the fabrication methods. It is found in our earlier study that for the typical operating conditions and physical parameters, the optimum catalyst thickness ranges from 10 to 15 μm [18]. Furthermore, scanning electron micrograph (SEM) of membrane electrode assembly shows that the catalyst layer thickness is around 10–20 μm and the mean agglomerate diameter is about 6 μm [22]. The operating parameters and the physical properties used in the numerical computation are listed in Table 1.

It is worthwhile to note that the bulk diffusion coefficient of oxygen is calculated according to the following relation [39]:

$$D_{\mathrm{O_2,bulk}} = \frac{1 - X_{\mathrm{O_2}}}{(X_{\mathrm{N_2}}/D_{\mathrm{O_2-N_2}}) + (X_{\mathrm{H_2O}}/D_{\mathrm{O_2-H_2O}})} \tag{23}$$

where $X_{\mathrm{O_2}}$, $X_{\mathrm{N_2}}$, and $X_{\mathrm{H_2O}}$ are the mole fractions of oxygen, nitrogen, and water vapor, respectively. The binary diffusion coefficient of oxygen and nitrogen, $D_{\mathrm{O_2-N_2}}$, is calculated using the Chapman-Enskog formula and the binary diffusion coefficient of oxygen and water vapor, $D_{\mathrm{O_2-H_2O}}$, is calculated using the Slattery-Bird equation [39,40]. Since the catalyst agglomerate is a mixture of electrolyte membrane, solid catalyst, and

Table 1
The operating and physical parameters in the present model calculations [10,18]

Parameter	Value
Operating temperature, T (°C)	50 and 80
Operating pressure, P (atm)	1 and 3
Electrode thickness, δ_e (μm)	250
Catalyst layer thickness, δ_c (μm)	10
Agglomerate diameter (μm)	5
Void fraction of the cathode electrode, ϕ_e	0.4
Fraction of membrane in the agglomerate, l_m	0.4
Fraction of flooding in the agglomerate, l_l	0.5
Catalyst loading per unit area, m_{Pt} (mg cm^{-2})	0.2
Fraction of catalyst, f_{Pt}	0.2
Catalyst surface area per unit mass of the catalyst, A_s (m^2 g^{-1})	112
Membrane conductivity, σ_m (S cm^{-1})	0.17
Solid catalyst conductivity, σ_s (S cm^{-1})	727
Density of platinum, ρ_{Pt} (g cm^{-3})	21.5
Density of carbon black, ρ_c (g cm^{-3})	2.0
Anodic transfer coefficient, α_a	0.5
Cathodic transfer coefficient, α_c	0.5

void region filled with liquid water and water vapor, the overall diffusion coefficient in the catalyst layer can be estimated using the following relation:

$$\frac{1}{D_{O_2-c}} = \frac{l_m}{D_{O_2-m}} + \frac{l_l}{D_{O_2-H_2O_{(l)}}} + \frac{l_g}{D_{O_2-H_2O_{(g)}}} \quad (24)$$

where l_m, l_l, and l_g are the fractions of membrane, liquid water, and water vapor in the catalyst agglomerate, respectively.

3. Numerical technique

The governing equations, Eqs. (3), (13), and (14) for inside and Eq. (3) for outside of the agglomerates, were solved subjected to the boundary conditions mentioned in the previous section. It should be pointed out that two approaches exist in literature for the numerical modeling of a fuel cell. In the first approach, current densities can be solved numerically by specifying overpotentials, and in the second approach, overpotentials are solved by specifying current densities. In the present work, the second approach was used.

The finite element method using COMSOL Multiphysics ™ running on a 64-bit Linux CPU with 3 GB of RAM was used. The computational domain was initially discretized into a tetrahedral mesh and Lagrangian elements of second order (quadratic elements) were used. Stationary nonlinear solver was chosen to solve the governing partial differential equations (PDEs). Since the governing PDEs are highly nonlinear, the general form of solution was chosen with the GMRES iterative solver and the geometric multigrid or SSOR techniques were used as pre-conditioners. Furthermore, governing equations are coupled together with the reaction rate term, hence, in the solution methodology an initial solution first obtained in a lower mesh and then the governing equations were solved individually at the higher level of mesh. The solutions were considered as converged solution when the preset tolerance value goes below 10^{-6} for each case. Detail description of the solver, the preconditioners, and the error estimation used in this study can be found in the COMSOL Multiphysics ™ user's guide [41].

3.1. Numerical validation

As mentioned earlier, none of the previous studies has considered the three-dimensional agglomerate arrangements; hence, direct comparison is not possible. Rather a limiting case of agglomerate model has been invoked for the validation of the accuracy of three-dimensional numerical calculation, where agglomerates are considered in a cylindrical computational domain. The advantage of using such three-dimensional domain is it can be solved as two-dimensional axi-symmetric problem, hence, the accuracy of the three-dimensional calculation can easily be verified with two-dimensional calculation. The thickness of the catalyst layer is chosen as 10 μm and the agglomerate diameter as 5 μm, i.e., two agglomerates can exist along the thickness of the catalyst layer. A schematic diagram of the three-dimensional computational domain and corresponding axi-symmetric computational domain used for the validation is shown in Fig. 2 along with the coordinate systems. Here, the number of agglomerates was kept as two, however, to maintain sufficient contact between the agglomerates, between the agglomerates and GDL, and between the agglomerates and membrane, the size of the each agglomerate has been increased by 2% keeping the centers of the agglomerates fixed. Boundary conditions for both the axi-symmetric model and the three-dimensional model were identical as described earlier.

Fig. 3 shows the oxygen concentration profile across the catalyst layer thickness along the centerline of the agglomerates (line OO′ in Fig. 2) for two current densities as indicated in the legend.

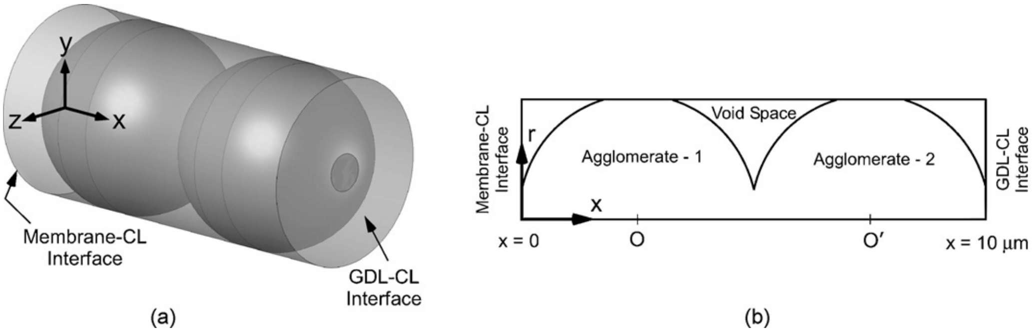

Fig. 2. Schematic of the computational domain: (a) three-dimensional domain, (b) two-dimensional axi-symmetric domain.

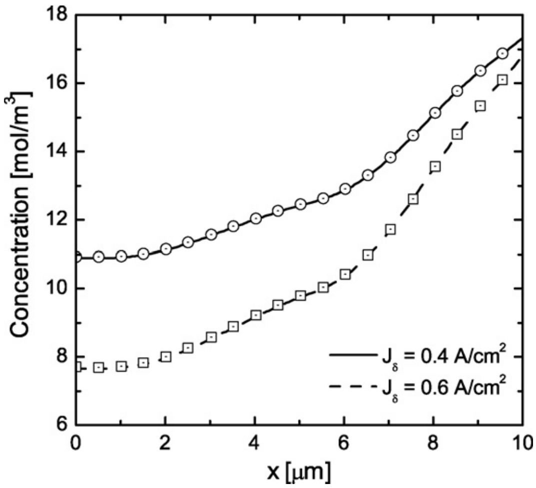

Fig. 3. Oxygen concentration profile in the cathode catalyst layer along the *x*-axis shown in Fig. 2 in a PEM fuel cell operating at 80 °C and 3 atm. Lines represent the axi-symmetric model results, whereas the symbols represent the three-dimensional model results of the present investigation for two current densities as indicated in the legend.

The operating pressure and temperature of the fuel cell is considered as 3 atm and 80 °C, respectively. The numerical procedure for the three-dimensional models is similar as described earlier. However, for axi-symmetric model, the advantage of adaptive mesh refinement technique has been employed for better accuracy. Conversely, Fig. 4 depicts the activation polarization for the three-dimensional model and the axi-symmetric model. As observed in Fig. 3 for both current densities, numerical solution of the three-dimensional model shows good agreement with the axi-symmetric model results. Furthermore, the activation polarization results also show excellent agreement. The accuracy of the two-dimensional finite element model using adaptive mesh refinement with commercial software, like COMSOL Multiphysics ^{TM}, is well-established [34,42]. Furthermore, two-dimensional numerical model required less number of grid to represent the curve surfaces. Whereas, three-dimensional models required significantly large number of gird for proper representation of spherical surfaces that is limited by computer memory. This limitation of computer memory eventually lower the accuracy of the three-dimensional numerical calculation. Since the comparisons shown here provide a good agreement with each other, it can easily be concluded that the three-dimensional model results presented in this study are sufficiently accurate for studying the effect of catalyst layer structures on the performance of PEM fuel cells. Once again, these results show the accuracy level of three-dimensional numerical computation, whereas the accuracy of the mathematical formulation has already been established elsewhere [18].

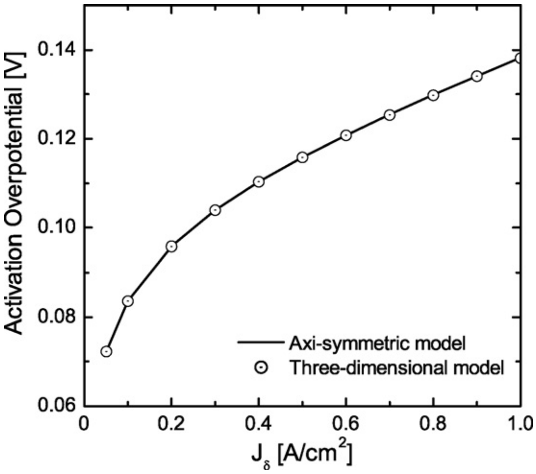

Fig. 4. Activation polarization of a PEM fuel cell operating at 80 °C and 3 atm. Lines represent the axi-symmetric model results, whereas the symbols represent the three-dimensional model results of the present investigation.

3.2. Grid sensitivity

In addition to the validation shown in the previous section, a comprehensive grid sensitivity test has been performed for all the three cases (Case-I, Case-II, and Case-III) to ensure the results are independent of grid sizes. This test also ensures the number of grid used in the three-dimensional numerical calculation is sufficient. The schematic of the agglomerate arrangement in the cathode catalyst layer and the computational domain for the three cases used in the present investigation is shown in Fig. 5. Here, Case-I represents in-line agglomerate arrangement, whereas Case-II and Case-III depict two staggered arrangements (uni-directional and bi-directional staggered arrangements). The orientation of the catalyst agglomerates in the catalyst layer for different agglomerate arrangements are listed in Table 2. Different level of meshes have been considered starting from approximately 0.4 million to 1 million degrees of freedom (DOF) for the three-dimensional models. These types of geometry cannot be solved as axi-symmetric, therefore, full three-dimensional computational domain is used to estimate oxygen concentrations and activation overpotentials. For illustration purpose, the grid sensitivity results are shown for Case-I only. Fig. 6 illustrates the variation of the oxygen concentration and the activation overpotential in the cathode catalyst layer along the centerline of the two reference agglomerates for Case-I. As mentioned earlier for Case-I, agglomerate arrangements are in-line in all directions, hence, the geometry is almost identical to three-dimensional domain shown in Fig. 2a, except the outer domain is rectangular instead of cylindrical. All the simulation parameters are identical to those for Fig. 4. Accuracy of the three-dimensional model has already been validated in Figs. 3 and 4, therefore, these results can be as accurate as Figs. 3 and 4. From Fig. 6, it

Table 2
Agglomerates orientation in different directions for the cases considered in the present investigation

	x-Direction	*y*-Direction	*z*-Direction
Case-I	In-line	In-line	In-line
Case-II	In-line	Staggered	In-line
Case-III	In-line	Staggered	Staggered

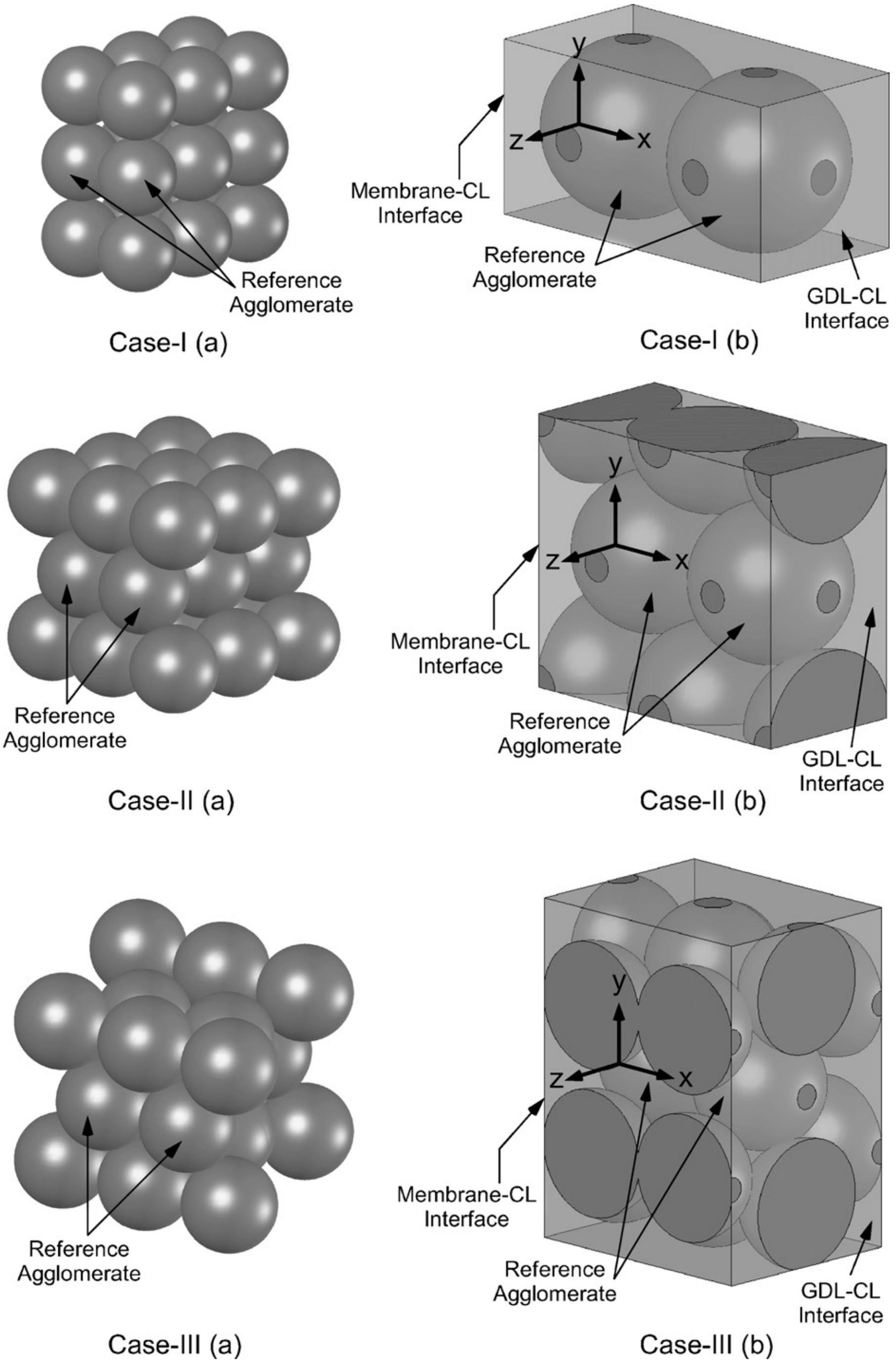

Fig. 5. Schematic of the agglomerate arrangements in the cathode catalyst layer in part (a) and the computational domain in part (b). Case-I represents in-line agglomerate arrangement, Case-II represents staggered arrangement in *y*-direction, and Case-III depicts staggered arrangement in both *y*- and *z*-directions.

is observed that all three grid levels show identical results. A close inspection of these results show about 0.5% variation in the oxygen concentration and about 0.2% variation in the activation overpotential between the highest and the lowest level meshes. Nevertheless, results shown in Fig. 6 are almost independent of the grid sizes. Since the Case-II and Case-III consist more spherical surfaces than the Case-I and also for better accuracy, results are presented for the highest grid level (approximately 1 million DOF) in all the subsequent figures.

4. Results and discussion

The accuracy of the three-dimensional finite element calculations has already been shown in the previous section by comparing three-dimensional model results with a two-dimensional axi-symmetric model, as well as results were compared for the grid sensitivity for the three different grid levels. In this section, results of a parametric study with three-different catalyst agglomerate arrangements are presented. As shown in Fig. 5, in Case-I, the catalyst agglomerates are con-

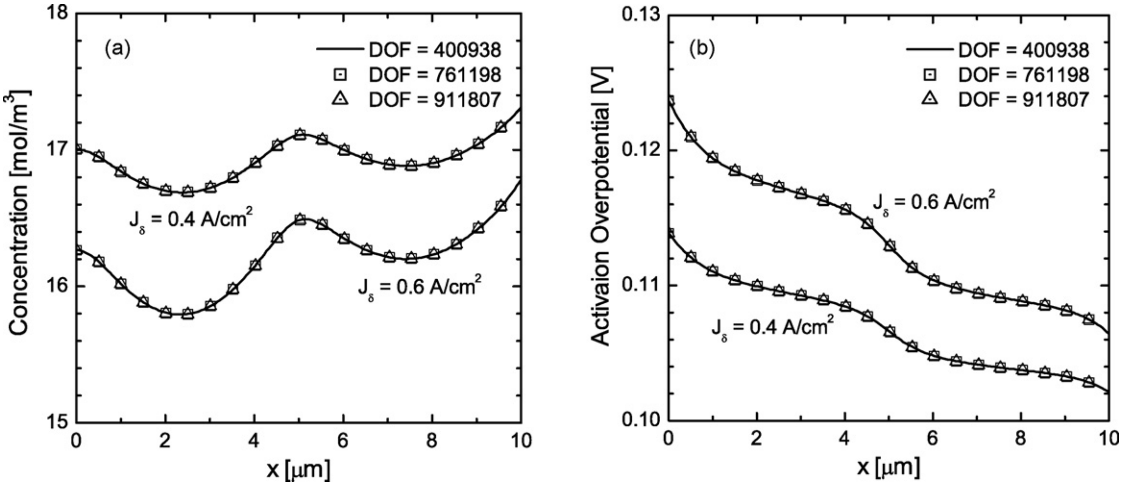

Fig. 6. Variation of oxygen concentration in the cathode catalyst layer along *x*-axis for Case-I in a PEM fuel cell operating at 80 °C and 3 atm in part (a) and the corresponding variation of the activation overpotential in part (b) for two current density values ($J_\delta = 0.4\,\mathrm{A\,cm^{-2}}$ and $0.6\,\mathrm{A\,cm^{-2}}$). Lines represent the results at the lowest degrees of freedom (DOF), whereas the symbols represent the results of two highest degrees of freedom as indicated in the figure.

sidered as in-line arrangement in all directions. For Case-II and Case-III, two staggered arrangements are considered as shown in Fig. 5. Here, staggered arrangement is considered in *y*-direction for Case-II, and for Case-III, both *y*- and *z*-directions have staggered arrangements of the catalyst agglomerates. For all the cases, *x*-direction is considered as in-line arrangement to keep symmetry between these cases. Due to the symmetry in *x*-direction, all the results are presented along the centerline between the two reference agglomerates (lied on the *x*-axis) as shown in part (b) of Fig. 5.

4.1. Case-I (in-line arrangement)

Fig. 7 shows the profiles of oxygen concentration with different current density values for Case-I. Each of these profiles is plotted inside the reference agglomerates along the *x*-axis that is identical of line OO$'$ as shown in Fig. 2. Five different current density values were considered as indicated in the legend. In both figures, the symbols represent the oxygen concentration profile along a line parallel to the *x*-axis at $y = 0$ and $z = 2.5\,\mu\mathrm{m}$ (equal to agglomerate radius) for $J_\delta = 0.1\ \mathrm{A\,cm^{-2}}$, i.e., along the interface between two agglomerates on *xz*-plane. The simulation parameters used to estimate the oxygen concentration are listed in Table 1. Two parts of this figure depict two different combinations of operating parameters, namely, $T = 50\,^\circ\mathrm{C}$ and $P = 1$ atm, and $T = 80\,^\circ\mathrm{C}$ and $P = 3$ atm. Here $x = 0$ represents the membrane–CL interface and $x = 10\,\mu\mathrm{m}$ represents the GDL–CL interface. It is observed that the oxygen concentration decreases along the centerline from the GDL–CL interface to the membrane–CL interface. For low current densities, the variation in the concentration is less whereas for high current densities an oscillatory behavior is observed in the profile. As expected, the minimum oxygen concentration is observed at the center point of the agglomerate and the two undulations in the profiles represent the two agglomerates. Although the concentration profile shows a decreasing behavior, significant amount

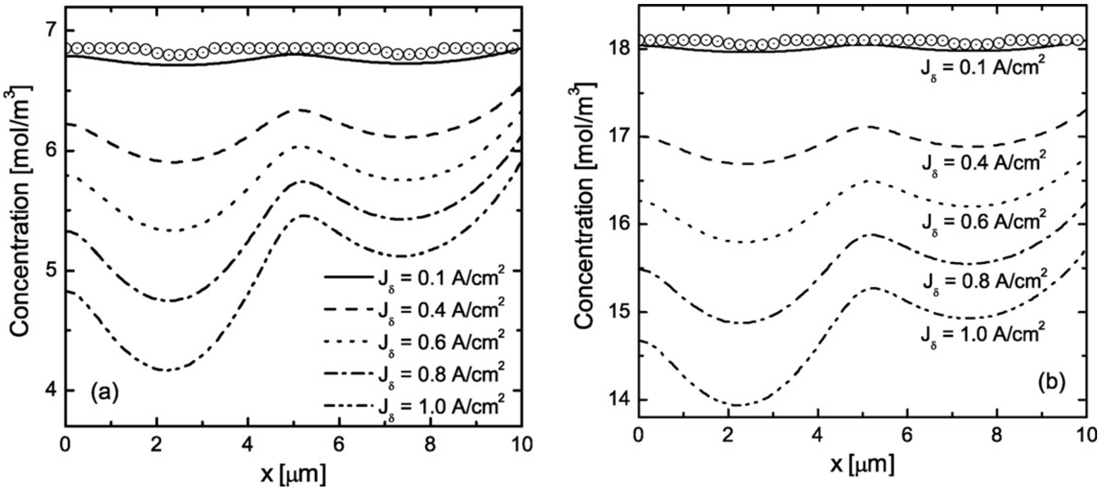

Fig. 7. Oxygen concentration profile in the cathode catalyst layer along the center line (*x*-axis in Fig. 5) of the agglomerates for Case-I in a PEM fuel cell operating at (a) $T = 50\,^\circ\mathrm{C}$ and $P = 1$ atm, and (b) $T = 80\,^\circ\mathrm{C}$ and $P = 3$ atm. Each line represents result of different current density values as indicated in the legend, while the symbols show the oxygen profile along a line parallel to *x*-axis at $y = 0$ and $z = 2.5\,\mu\mathrm{m}$ for $J_\delta = 0.1\ \mathrm{A\,cm^{-2}}$. All other parameters are listed in Table 1.

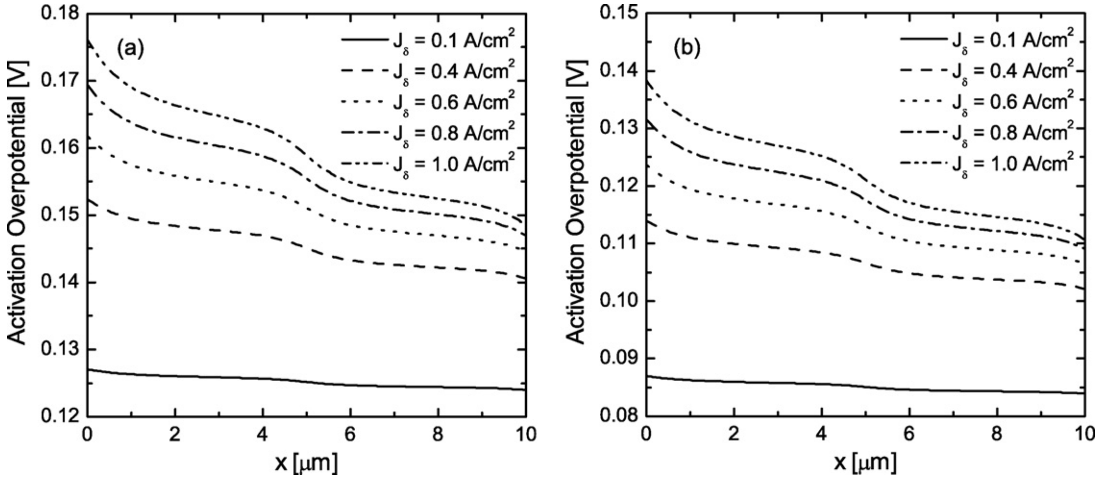

Fig. 8. Distribution of the activation overpotential in the cathode catalyst layer for Case-I corresponding to the oxygen concentration shown in Fig. 7. Each line represents different current density values as indicated in the legend while part (a) for $T = 50\,^{\circ}\mathrm{C}$ and $P = 1$ atm, and part (b) for $T = 80\,^{\circ}\mathrm{C}$ and $P = 3$ atm.

of oxygen concentration still exists in the membrane–CL interface due to the fast oxygen diffusion through the void region around the catalyst agglomerates. Further, in this study, an ideal case scenario is considered when there is no flooding outside the catalyst agglomerates, whereas the catalyst agglomerates are partially flooded. Hence, oxygen diffusion across the dry void region dominates over the diffusion through the partially flooded catalyst agglomerates as shown by symbols in both figure for $J_\delta = 0.1\,\mathrm{A\,cm^{-2}}$. Here, oxygen concentration is almost constant in the void region along x-axis due to the favorable oxygen transport. Only variation is observed at the contact surfaces between the reference and surrounding agglomerates. Since no variation is observed in the oxygen concentration profile, in subsequent figures, results in the void region have not been reported. It is also clear from Fig. 7 that in the agglomerate, oxygen is transported in two ways: first oxygen diffuses along the axial direction or the thickness of the catalyst layer in the void region, then from the void region, oxygen diffuses in the radial direction towards the center of the each agglomerate.

In Fig. 8, the cathode activation overpotential is plotted as a function of spatial coordinate x in the catalyst layer for different current density values as indicated in the legend. Similar to Fig. 7, two parts show two different combinations of the operating parameters as indicated in the figure. Each line corresponds to the activation overpotential for the oxygen concentration shown in Fig. 7. Identical to the concentration profile, the variation of the activation overpotential in the catalyst layer is small at low current densities, whereas the activation overpotential decreases rapidly from the membrane–CL interface to the GDL–CL interface for the higher current densities. For all the current densities, the activation overpotential is higher for lower pressure and temperature than the overpotential for the higher pressure and temperature. This is mainly due to the fast oxygen transport in the catalyst layer at $80\,^{\circ}\mathrm{C}$ and 3 atm.

Fig. 9 illustrates the variations of the reaction rate in the catalyst layer corresponding to the oxygen concentration and the activation overpotential shown in Figs. 7 and 8, respectively, for five different current densities. Here, the lines represent the results for $T = 50\,^{\circ}\mathrm{C}$ and $P = 1$ atm, and the symbols are $T = 80\,^{\circ}\mathrm{C}$ and $P = 3$ atm. Surprisingly, changing the operating condition does not show any significant effect on the reaction rate. However, slightly higher reaction rate is observed for $T = 80\,^{\circ}\mathrm{C}$ and $P = 3$ atm at the center of the agglomerates for high current densities. These similarities show that the rate of the electro-chemical reaction is not responsible for the difference observed in the activation overpotential in Fig. 8 for different operating conditions, which is solely due to the variation of oxygen concentration in the catalyst layer. Although the reactions are faster at higher temperatures and pressures, here it has not been significantly observed since a higher operating temperature and pressure is known to reduce the activation overpotential which is the driving force for the electro-chemical reactions occurring in the fuel cells.

4.2. Case-II (staggered arrangement-I)

For the staggered arrangements of catalyst agglomerates, two cases were considered. In the first staggered arrangement, agglomerates were considered as staggered in y-direction, i.e.,

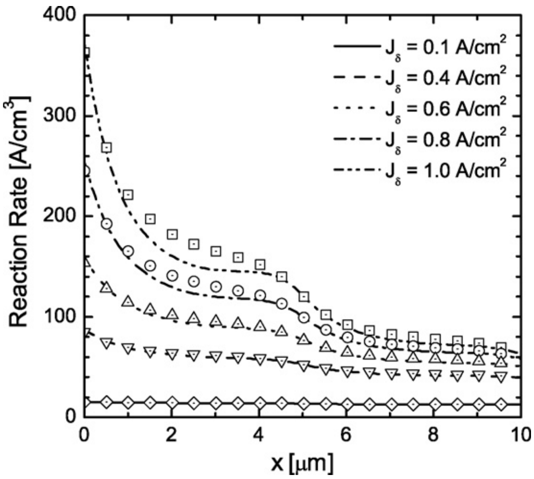

Fig. 9. Variation of the reaction rate in the cathode catalyst layer along x-axis for Case-I. Lines represent the results for operating conditions of $T = 50\,^{\circ}\mathrm{C}$ and $P = 1$ atm, and the symbols depict the corresponding results for $T = 80\,^{\circ}\mathrm{C}$ and $P = 3$ atm.

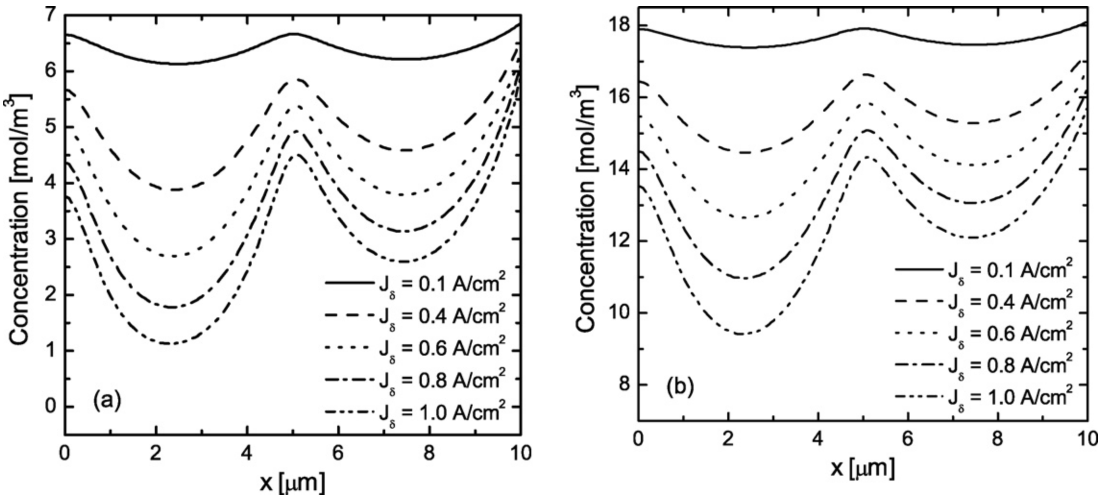

Fig. 10. Oxygen concentration profile in the cathode catalyst layer along *x*-axis for Case-II in a PEM fuel cell operating at: (a) $T = 50\,^\circ\mathrm{C}$ and $P = 1$ atm, and (b) $T = 80\,^\circ\mathrm{C}$ and $P = 3$ atm. Each line represents result of different current density values as indicated in the legend. All other parameters are same as Case-I.

uni-directional staggered arrangement, as shown in Fig. 5 as Case-II. To maintain a similarity with Case-I, the thickness of the catalyst layer is kept 10 μm. Here, the reference agglomerates (lied on the *x*-axis) are considered as spherical, whereas the surrounding agglomerates can be either spherical or hemispherical to maintain the thickness of the catalyst layer same for all cases. All the model results for this case (Case-II) are also presented along the centerline of the two middle agglomerates, i.e., along the *x*-axis. The oxygen concentration profile in the catalyst layer for Case-II is shown with different current density values in Fig. 10. All the simulation parameters are identical of Case-I. Results of two different combination of operating parameters, namely, $T = 50\,^\circ\mathrm{C}$ and $P = 1$ atm, and $T = 80\,^\circ\mathrm{C}$ and $P = 3$ atm are shown in Fig. 10 a and b, respectively. Although the oxygen concentration at the interface of GDL–CL for similar temperature and pressure are equal for both Case-I and Case-II; for Case-II, a smaller value of oxygen concentration is observed at the interface of membrane–CL. This is reasonable, since in Case-II, agglomerates are staggered in *y*-direction. Hence, Case-II has less void space around the agglomerates compared to Case-I, which eventually prevents faster oxygen diffusion through the constricted void spaces. Furthermore, the undulatory profile in the oxygen concentration is more prominent in this case. Qualitatively, oxygen concentration profile for both the pressure and temperature combinations show similar behavior except their magnitudes. Further inspection on the values of oxygen concentration at the GDL–CL interface shows that at higher temperature and pressure, concentration is higher than the smaller temperature and pressure combination. This is mainly due to the faster transport processes through the un-flooded GDL at higher pressure and temperature, though oxygen concentration in the gas channel is less for $T = 80\,^\circ\mathrm{C}$ and $P = 3$ atm due to the higher fraction of water vapor. Irrespective to the magnitude of the oxygen concentration in the catalyst layer, temperature and pressure does not show any significant effect on the profile of oxygen concentration in the catalyst layer.

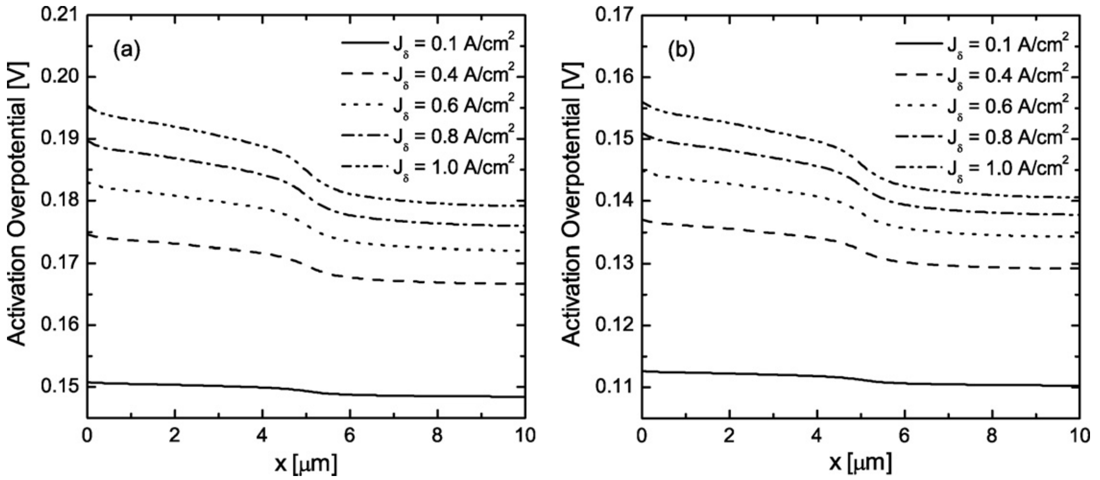

Fig. 11. Distribution of the activation overpotential in the cathode catalyst layer for Case-II corresponding to the oxygen concentration shown in Fig. 10. Each line represents different current density values as indicated in the legend while part (a) for $T = 50\,^\circ\mathrm{C}$ and $P = 1$ atm, and part (b) for $T = 80\,^\circ\mathrm{C}$ and $P = 3$ atm.

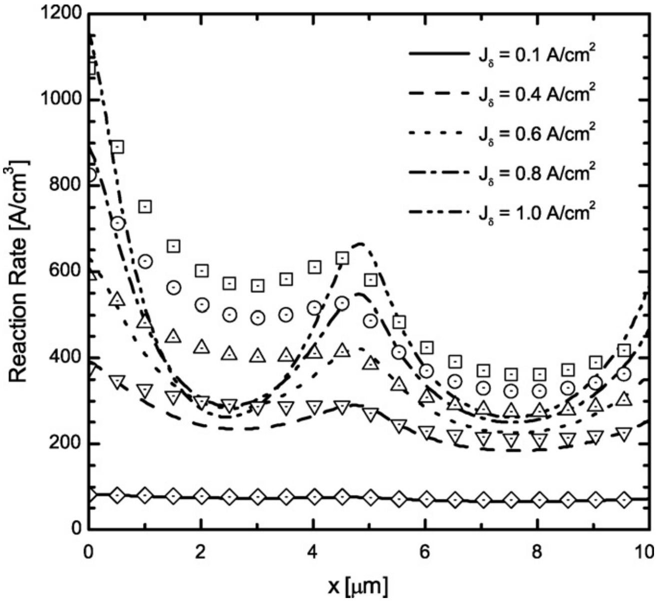

Fig. 12. Variation of the reaction rate in the cathode catalyst layer along *x*-axis for Case-II. Lines represent the results for operating conditions of $T = 50\,^{\circ}\mathrm{C}$ and $P = 1$ atm, and the symbols represent the corresponding results for $T = 80\,^{\circ}\mathrm{C}$ and $P = 3$ atm.

The variations observed here is mainly due to the catalyst layer structures, or in the other words, operating conditions dictate the quantity in the transport process whereas agglomerate structures dictate the quality of the diffusion in the transport processes.

Similar to the Case-I, the results of Case-II for $T = 50\,^{\circ}\mathrm{C}$ and $P = 1$ atm show higher activation overpotential than the corresponding overpotential for $T = 80\,^{\circ}\mathrm{C}$ and $P = 3$ atm as shown in Fig. 11. Comparing Fig. 11 with Fig. 8 reveals higher activation loss for staggered agglomerate arrangements, since lesser path available for the oxygen transport due to the staggered agglomerate orientation in the catalyst layer. The variation of the reaction rate in the cathode catalyst layer for the Case-II is shown in Fig. 12. Here, the lines represent the results for $T = 50\,^{\circ}\mathrm{C}$ and $P = 1$ atm, and the symbols represent results corresponding to $T = 80\,^{\circ}\mathrm{C}$ and $P = 3$ atm for five current densities as indicated in the legend. Here a distinct difference is observed in the reaction rate profile in two operating conditions. For higher temperature and pressure, the rate of reaction is higher nearby the center of the agglomerates at high current density values. An undulatory nature has been observed in the reaction rate profile, while a crest exists at the interface between the two reference agglomerates. This undulatory behavior is more prominent in higher operating parameter values and high current densities. Furthermore, in some instance, the higher current density shows lower reaction rate at the center of the agglomerates for $T = 50\,^{\circ}\mathrm{C}$ and $P = 1$ atm, which might be due to insufficient oxygen available on the surface of the agglomerates or slow diffusion towards the center of the agglomerates at higher current densities.

4.3. *Case-III (staggered arrangement-II)*

In the second type of staggered arrangement, the arrangements of catalyst agglomerates were considered as staggered in *y*- and *z*-directions, i.e., bi-directional staggered arrangement, as shown in Fig. 5 as Case-III. Like the other two cases, all the results are presented along the centerline of the two reference agglomerates that is along *x*- axis (see Case-III in Fig. 5). Fig. 13 shows the variations of the oxygen concentration with different current density values as indicated in the legend for $T = 50\,^{\circ}\mathrm{C}$ and $P = 1$ atm (Fig. 13a), and $T = 80\,^{\circ}\mathrm{C}$ and $P = 3$ atm (Fig. 13b). The oxygen concentration profiles show almost identical behavior like Case-II. However, at the center of the agglomerates, oxygen concentration is slightly higher than the Case-II. Since the Case-III has staggered structures of agglomerate arrangements in two directions, the diffusion around the agglomerates is non-uniform. This non-uniformity eventually provides favorable environment for the oxygen diffusion in the radial direction of the agglomerates for Case-III. Furthermore, better oxygen diffusion also reduces the activation overpotential for the Case-III as shown in Fig. 14 for both operating conditions compared to the Case-II. This can be better explained by visualizing the agglomerate arrangements. For Case-II, staggered arrangement exists in one direction, therefore, oxygen diffusion outside the agglomerates is faster in the direction where in-line arrangements exist, and slower in the staggered direction. When it comes to the agglomerates surface, then more oxygen is available in certain areas, whereas not all oxygen can diffuse inside the agglomerate through the radial direction. This can be visualized by plotting oxygen concentration in the void region for Case-II and Case-III. Fig. 15 shows oxygen concentration profile outside the agglomerates along a line parallel to the *x*-axis at $y = 0$ and $z = 2.5\,\mu\mathrm{m}$ for $T = 80\,^{\circ}\mathrm{C}$ and $P = 3$ atm. Here, the lines depict results for Case-II and the symbols for Case-III for different current density values as indicated in the legend. As observed in Fig. 15, oxygen concentration on the catalyst surface for Case-III is higher than Case-II at the interfaces between two agglomerates ($2\,\mu\mathrm{m} < x < 3\,\mu\mathrm{m}$ and $7\,\mu\mathrm{m} < x < 8\,\mu\mathrm{m}$) for all the current density values. Therefore, more oxygen available for Case-III to diffuse in the *y*-direction that is due to the staggered arrangements in the *z*-direction. Furthermore, due to the higher oxygen concentration in certain areas, diffusion will be faster for Case-III in *y*-direction. Also, due to the in-line arrangements in two directions, less oxygen available in certain areas on the agglomerate surface for Case-II whereas capacity of diffusion through the radial direction is more. When it comes to the diffusion through the individual agglomerate, all the geometries have same composition inside the agglomerate; hence, the entire diffusion processes is control by the amount of oxygen available at the surface of the agglomerates and how the concentration is distributed over the agglomerate surfaces. In other words, capacity of the diffusion is higher than the amount of oxygen available on the agglomerate surfaces for Case-II. Combining these effects eventually lower the oxygen concentration at the agglomerate center in Case-II (see Fig. 10). For Case-III, since staggered structures exist in two directions, available oxygen on the surface of the agglomerates is higher in the *y*-direction than Case-II. This eventually enhances the diffusion process in the radial direction due to the higher oxygen availability and lowers the activation overpotential as shown in Fig. 14. It might

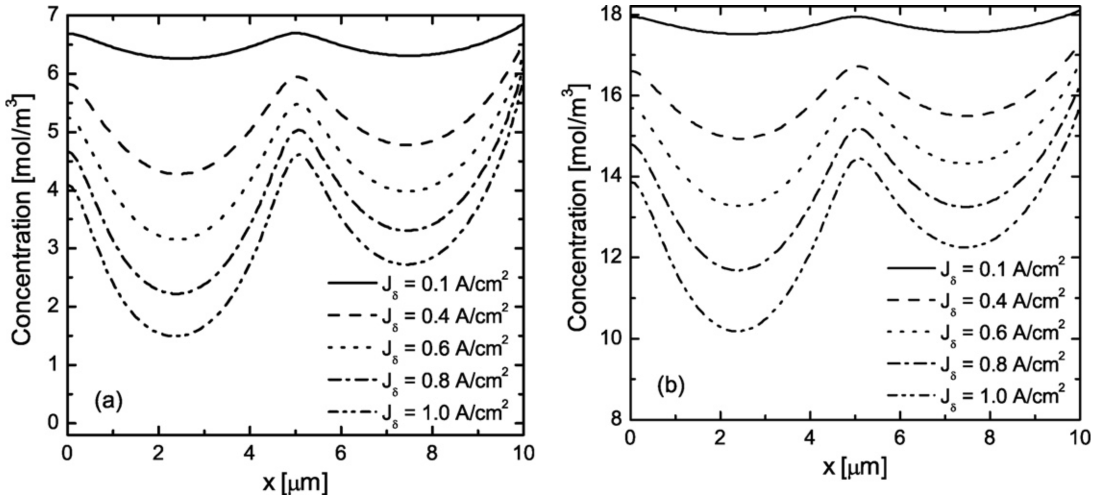

Fig. 13. Oxygen concentration profile in the cathode catalyst layer along the *x*-axis for Case-III in a PEM fuel cell operating at: (a) $T = 50\,^\circ$C and $P = 1$ atm, and (b) $T = 80\,^\circ$C and $P = 3$ atm. Each line represents result of different current density values as indicated in the legend.

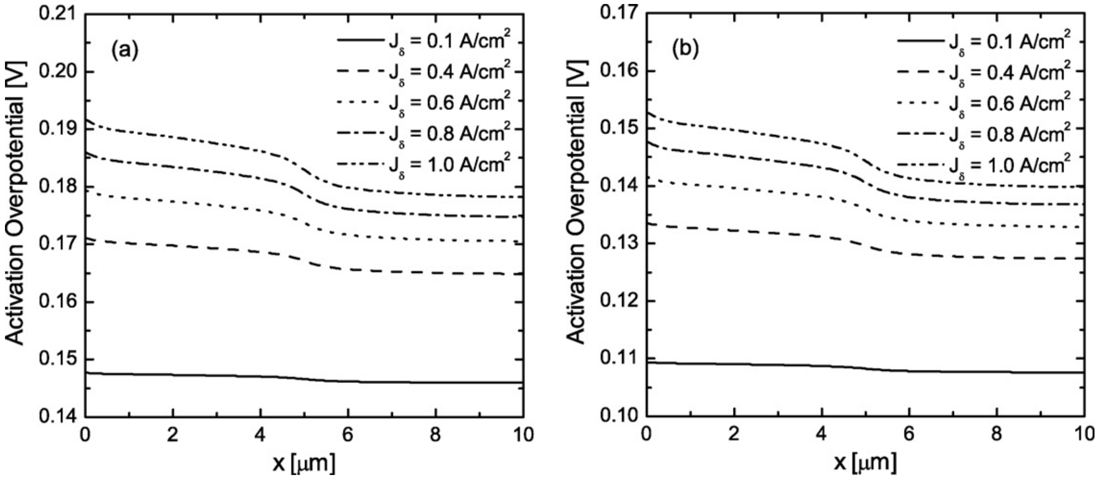

Fig. 14. Distribution of the activation overpotential in the cathode catalyst layer for Case-III corresponding to the oxygen concentration shown in Fig. 13. Each line represents different current density values as indicated in the legend while part (a) for $T = 50\,^\circ$C and $P = 1$ atm, and part (b) for $T = 80\,^\circ$C and $P = 3$ atm.

be questionable, though Case-III has higher non-uniformity in the catalyst arrangements then why Case-III show better diffusion results. The simple answer will be it provides better passage in the void region in *z*-direction due to the staggered arrangements.

In the reaction rate of Case-III, similar behavior is observed like Case-II. The plot of the reaction rate for Case-III is shown in Fig. 16 for $T = 50\,^\circ$C and $P = 1$ atm as lines, and for $T = 80\,^\circ$C and $P = 3$ atm as symbols. For all the current densities, the reaction rate is higher for higher operating parameters and lower for lower operating parameters. The local variation in the reaction rate observed here mainly due to the local change of oxygen concentration observed in Fig. 13 for different operating conditions. Like the activation overpotential, the rate of reaction is also lower for Case-III compared to Case-II as shown in Fig. 17. In Fig. 17, the reaction rates are plotted for all the three cases along the *x*-axis for $J_\delta = 0.6$ A cm^{-2} for the fuel cell operating at $T = 80\,^\circ$C and $P = 3$ atm. For the entire thickness of the catalyst layer, reaction rate is highest for the Case-II and

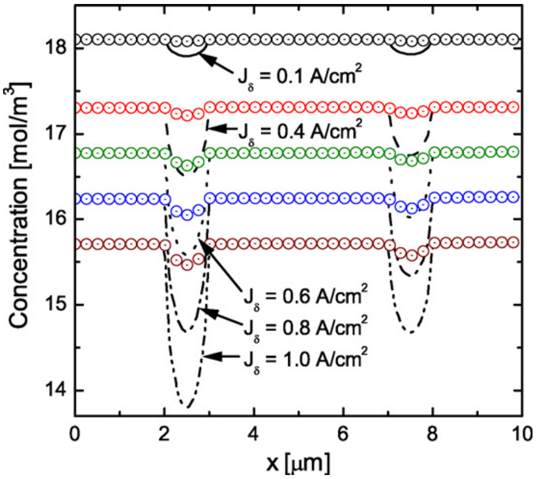

Fig. 15. Oxygen concentration profile in the cathode catalyst layer along a line parallel to *x*-axis at $y = 0$ and $z = 2.5$ μm for $T = 80\,^\circ$C and $P = 3$ atm. Lines represent the result for Case-II, while the symbols represent Case-III for five different current density values as indicated in the legend.

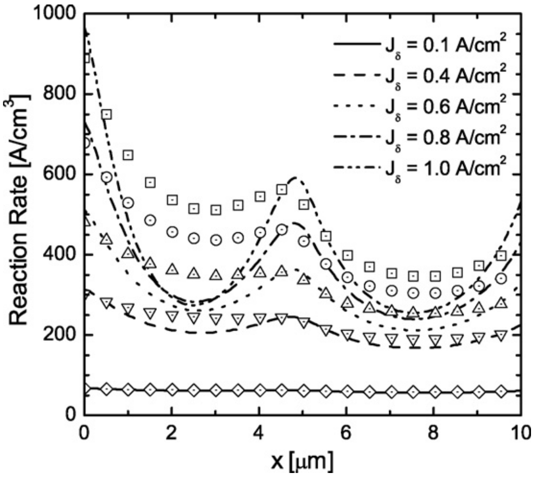

Fig. 16. Variation of the reaction rate in the cathode catalyst layer along *x*-axis for Case-III. Lines represent the results for operating conditions of $T = 50\,^\circ$C and $P = 1$ atm, and the symbols represent the results for $T = 80\,^\circ$C and $P = 3$ atm.

lowest for the Case-I. This might be another possible cause for the lower oxygen concentration observed at the center of the agglomerates for Case-II (*cf.* Fig. 10) compared to Case-III. In addition, concentration, reaction rate, and activation overpotential are coupled; therefore, it is required to optimize those variables in order to find better cell performance and design. Nevertheless, the results obtained from the present investigation reveals a considerable insight on how the governing parameters for PEM fuel cells change with the structures of the catalyst layer as well as with the operating conditions. Like the Case-II shows highest reaction rate that means the speed of the chemical reaction is faster, hence less catalyst will be required to promote the electro-chemical reaction. On the other hand, Case-II also shows higher activation losses. Therefore, the results presented in this paper providing information, and the direction when and where the optimization is possible or at what extent it is possible.

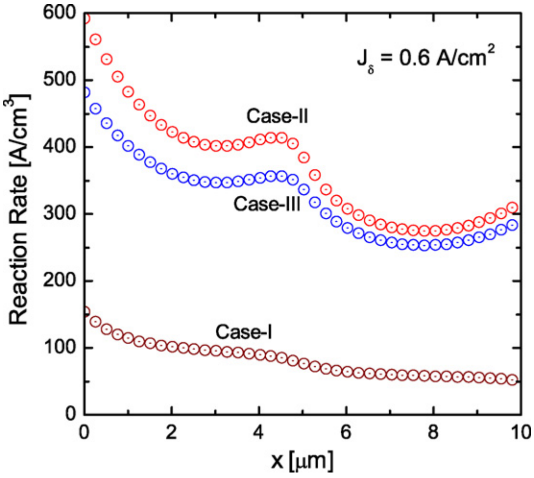

Fig. 17. Comparison between the reaction rates at $J_\delta = 0.6\,\mathrm{A\,cm^{-2}}$for the fuel cell operating at $T = 80\,^\circ$C and $P = 3$ atm. Each line represents the reaction rate along the *x*-axis for three cases as indicated in the legend.

5. Conclusions

In this paper, a three-dimensional agglomerate model for the cathode catalyst layer in a PEM fuel cell has been developed to study the effect of catalyst agglomerate arrangements. A comprehensive validation has also been shown that indicates complex staggered arrangement of catalyst agglomerates in three-dimensional catalyst layer modeling is possible. Considering the three different arrangements of catalyst agglomerates investigated here, it is found that the agglomerate arrangements in the catalyst layer have significant effect on the oxygen transport processes in the catalyst layer, consequently the activation losses and the rate of reactions. Therefore, in the fuel cell modeling, detailed catalyst layer structures should be considered to capture the true nature of the PEM fuel cell performance, particularly, its activation losses. It has also been observed that in-line arrangement of the catalyst agglomerates yields lowest activation loss, although in reality catalyst agglomerates may be staggered in all directions. For example, almost 17% of reduction in the activation overpotential is possible by using in-line arrangement of the catalyst agglomerates at the current density of $0.4\,\mathrm{A\,cm^{-2}}$ for $T = 80\,^\circ$C and $P = 3$ atm. Among the two staggered arrangements, bi-directional (Case-III) staggered arrangement shows less activation overpotential than uni-directional (Case-II) staggered arrangement. In fact, 3–4% of activation losses can be recovered (considering Case-II with Case-III) just by changing the agglomerate arrangements. Hence, it might be possible to identify an optimum catalyst layer structures by further investigating such staggered arrangements. Furthermore, it seems that the present catalyst layer models will be useful in optimizing the catalyst layer structures and catalyst distribution.

Acknowledgements

This study is financially supported by the Natural Sciences and Engineering Research Council of Canada (NSERC). One of the authors (P.K.D.) also acknowledges a financial support from the NSERC as Canada Graduate Scholarship.

References

[1] X. Li, Principles of Fuel Cells, Taylor & Francis, 2006.
[2] T.E. Springer, T.A. Zawodzinski, S. Gottesfeld, J. Electrochem. Soc. 138 (1991) 2334–2342.
[3] D.M. Bernardi, M.W. Verbrugge, AIChE J. 37 (1991) 1151–1163.
[4] D.M. Bernardi, M.W. Verbrugge, J. Electrochem. Soc. 139 (1992) 2477–2491.
[5] T.E. Springer, M.S. Wilson, S. Gottesfeld, J. Electrochem. Soc. 140 (1993) 3513–3526.
[6] J.C. Amphlett, R.M. Baumert, R.F. Mann, B.A. Peppley, P.R. Roberge, T.J. Harris, J. Electrochem. Soc. 142 (1995) 1–8.
[7] J.C. Amphlett, R.M. Baumert, R.F. Mann, B.A. Peppley, P.R. Roberge, T.J. Harris, J. Electrochem. Soc. 142 (1995) 9–15.
[8] J. Kim, S.M. Lee, S. Srinivasan, C.E. Chamberlin, J. Electrochem. Soc. 142 (1995) 2670–2674.
[9] M. Eikerling, A.A. Kornyshev, J. Electroanal. Chem. 453 (1998) 89–106.
[10] C. Marr, X. Li, J. Power Sources 77 (1999) 17–27.
[11] J.J. Baschuk, X. Li, J. Power Sources 86 (2000) 181–196.

[12] S. Dutta, S. Shimpalee, J.W. Van Zee, J. Appl. Electrochem. 30 (2000) 135–146.
[13] S. Dutta, S. Shimpalee, J.W. Van Zee, Int. J. Heat Mass Transfer 44 (2001) 2029–2042.
[14] A. Rowe, X. Li, J. Power Sources 102 (2001) 82–96.
[15] Q.P. Wang, D.T. Song, T. Navessin, S. Holdcroft, Z.S. Liu, Electrochim. Acta 50 (2004) 725–730.
[16] S. Shimpalee, S. Greenway, D. Spuckler, J.W. Van Zee, J. Power Sources 135 (2004) 79–87.
[17] D.T. Song, Q.P. Wang, Z.S. Liu, M. Eikerling, Z. Xie, T. Navessin, S. Holdcroft, Electrochim. Acta 50 (2005) 3347–3358.
[18] P.K. Das, X. Li, Z.S. Liu, J. Electroanal. Chem. 604 (2007) 72–90.
[19] M.S. Wilson, S. Gottesfeld, J. Appl. Electrochem. 22 (1992) 1–7.
[20] Y.W. Rho, S. Srinivasan, Y.T. Kho, J. Electrochem. Soc. 141 (1994) 2089–2096.
[21] M. Uchida, Y. Fukuoka, Y. Sugawara, N. Eda, A. Ohta, J. Electrochem. Soc. 143 (7) (1996) 2245–2252.
[22] K. Broka, P. Ekdunge, J. Appl. Electrochem. 27 (1997) 281–289.
[23] M.L. Perry, J. Newman, E.J. Cairns, J. Electrochem. Soc. 145 (1998) 5–15.
[24] N.P. Siegel, M.W. Ellis, D.J. Nelson, M.R. von Spakovsky, J. Power Sources 115 (2003) 81–89.
[25] K.M. Yin, J. Electrochem. Soc. 152 (2005) A583–A593.
[26] Q.P. Wang, M. Eikerling, D.T. Song, Z.S. Liu, J. Electroanal. Chem. 573 (2004) 61–69.
[27] W. Sun, B.A. Peppley, K. Karan, Electrochim. Acta 50 (2005) 3359–3374.
[28] G.Y. Lin, W.S. He, T. van Nguyen, J. Electrochem. Soc. 151 (2004) A1999–A2006.
[29] C.Y. Du, X.Q. Cheng, T. Yang, G.P. Yin, P.F. Shi, Electrochem. Commun. 7 (2005) 1411–1416.
[30] D.T. Song, Q.P. Wang, Z.S. Liu, T. Navessin, S. Holdcroft, Electrochim. Acta 50 (2004) 731–737.
[31] A. Fischer, J. Jindra, H. Wendt, J. Appl. Electrochem. 28 (1998) 277–282.
[32] T. Berning, D.M. Lu, N. Djilali, J. Power Sources 106 (2002) 284–294.
[33] Q.P. Wang, M. Eikerling, D.T. Song, Z.S. Liu, T. Navessin, Z. Xie, S. Holdcroft, J. Electrochem. Soc. 151 (2004) A950–A957.
[34] P.K. Das, S. Bhattacharjee, W. Moussa, Langmuir 19 (2003) 4162–4172.
[35] P.K. Das, S. Bhattacharjee, J. Colloid Interface Sci. 273 (2004) 278–290.
[36] D.A.G. Bruggeman, Ann. Phys. (Leipzig) 24 (1935) 636–679.
[37] A.Z. Weber, J. Newman, Chem. Rev. 104 (2004) 4679–4726.
[38] A. Parthasarathy, S. Srinivasan, A.J. Appleby, C.R. Martin, J. Electrochem. Soc. 139 (1992) 2530–2537.
[39] R.H. Perry, D.W. Green, Perry's Chemical Engineers' Handbook, McGraw-Hill, New York, 1997.
[40] R.B. Bird, W.E. Stewart, E.N. Lightfoot, Transport Phenomena, John Wiley & Sons Inc., New York, 1960.
[41] COMSOL Inc., User's Guide, Version 3.2a, 2006.
[42] P.K. Das, S. Bhattacharjee, Colloids Surf. A 256 (2005) 91–103.